Control Scheme and Networked Control Architecture for the Berkeley Lower Extremity Exoskeleton (BLEEX)[*]

Ryan Steger, Sung Hoon Kim, and H. Kazerooni

Department of Mechanical Engineering
University of California, Berkeley
Berkeley, CA 94720, USA
exo@me.berkeley.edu

Abstract − **The Berkeley Lower Extremity Exoskeleton (BLEEX) is a load-carrying and energetically autonomous human exoskeleton that, in this first generation prototype, carries up to a 34 kg (75 lb) payload for the pilot and allows the pilot to walk at up to 1.3 m/s (2.9 mph). This article focuses on the human-in-the-loop control scheme and the novel ring-based networked control architecture (ExoNET) that together enable BLEEX to support payload while safely moving in concert with the human pilot. The BLEEX sensitivity amplification control algorithm proposed here increases the closed loop system sensitivity to its wearer's forces and torques without any measurement from the wearer (such as force, position, or electromyogram signal). The tradeoffs between not having sensors to measure human variables, the need for dynamic model accuracy, and robustness to parameter uncertainty are described. ExoNET provides the physical network on which the BLEEX control algorithm runs. The ExoNET control network guarantees strict determinism, optimized data transfer for small data sizes, and flexibility in configuration. Its features and application on BLEEX are described.**

Index Terms − BLEEX, exoskeleton, human-machine, control, wearable robotics, ExoNet, bLAN, ring-based, networked control.

I. INTRODUCTION

The goal of the exoskeleton project at U.C. Berkeley is to develop fundamental technologies associated with the design and control of energetically autonomous lower extremity exoskeletons that augment human strength and endurance during locomotion. The first generation lower extremity exoskeleton (commonly referred to as BLEEX) is comprised of two powered anthropomorphic legs, a power unit, and a backpack-like frame on which a variety of heavy loads can be mounted. This system provides its pilot (i.e. the wearer) the ability to carry significant loads on his/her back with minimal effort over any type of terrain. BLEEX allows the pilot to comfortably squat, bend, swing from side to side, twist, and walk on ascending and descending slopes, while also offering the ability to step over and under obstructions while carrying equipment and supplies. BLEEX has numerous potential applications; it can provide soldiers, disaster relief workers, wildfire fighters, and other emergency personnel the ability to carry heavy loads such as food, rescue equipment, first-aid supplies, communications gear, and weaponry, without the strain typically associated with demanding labor.

Fig. 1 Berkeley Lower Extremity Exoskeleton (BLEEX) first generation prototype and pilot. 1: Hydraulic power supply and payload occupies the upper portion of the backpack; 2: Rigid BLEEX spine connected to the flexible pilot vest; 3: Central control computer occupies the lower portion of the backpack; 4: Some of the hydraulic actuators (ankle, knee and hip); 5: Two of the control network's Remote I/O Modules (RIOM); 6: Rigid connection of the BLEEX feet to the pilot's boots. More photographs can be found at http://bleex.me.berkeley.edu

BLEEX was first unveiled in 2004, at U.C. Berkeley's Human Engineering and Robotics Laboratory (Fig. 1). In this initial model, BLEEX offered a carrying capacity of 34 kg (75 lbs), with weight in excess of that allowance being supported by the pilot.

The effectiveness of the lower extremity exoskeleton is a direct result of the control system's ability to leverage the human intellect to provide balance, navigation, and path-planning while ensuring that the exoskeleton actuators provide most of the strength necessary for supporting payload and walking. In operation, the exoskeleton becomes transparent to the pilot and there is no need to train or learn any type of interface to use the robot.

3469

The control algorithm ensures that the exoskeleton always moves in concert with the pilot with minimal interaction force between the two and was first presented in [1]. It needs no direct measurements from the pilot or the human-machine interface (e.g. no force sensors between the two). The controller estimates, based on measurements from the exoskeleton structure only, how to move so that the pilot feels very little force. This control scheme is an effective method of generating locomotion when the contact location between the pilot and the exoskeleton is unknown and unpredictable (i.e. the exoskeleton and the pilot are in contact in variety of places).

This control method differs from compliance control methods employed for upper extremity exoskeletons [1], and haptic systems [2],[3] because it requires no force sensor between the wearer and the exoskeleton. Taking into account this new approach, our goal was to develop a control system for BLEEX with high sensitivity. High sensitivity brings two realistic concerns; the first was that an exoskeleton with high sensitivity to external forces and torques would respond to other external forces not initiated by its pilot. The pilot's ability to move quickly (e.g. step back or sideways) to create a stable situation for himself and the exoskeleton is the key to preventing the exoskeleton from falling in response to external forces. For this, a very wide control bandwidth is needed so the exoskeleton can respond to both pilot's voluntary and involuntary movements (i.e. reflexes).

The second concern is that systems with high sensitivity to external forces and torques are not robust to variations and therefore the precision of the system performance will be proportional to the precision of the exoskeleton dynamic model. To mitigate this drawback, we have employed system identification to validate model parameters, which is discussed in detail in [4]. Various experimental systems in our laboratory have in fact proved the overall effectiveness of the control method in shadowing the pilot's movement.

Realization of this control scheme requires a high-performance physical control architecture. This paper presents the ring-based protocol and distributed networked control hardware called the ExoNet. Traditional centralized control architectures where a supervisory controller directly interfaces in a point-to-point fashion with all sensors and actuators in the system have been successfully implemented in the past. They are generally feasible when a controller interfaces with small number of sensors and actuators and requires short wiring to them. Larger sophisticated multi-degree-of-freedom systems frequently require the control network to be compact, easily reconfigurable, expandable, and maintainable. Hence, we utilized a networked control system (NCS) as an alternative to the conventional centralized control system because of its advantages in flexibility, volume of wiring and capacity of distribution.

II. PREVIOUS WORK

In our research work at U.C. Berkeley, we have divided the technology associated with human power augmentation into lower extremity exoskeletons and upper extremity exoskeletons. The reason for this was two-fold; firstly, we could envision a great many applications for either a stand-alone lower or upper extremity exoskeleton in the immediate future. Secondly, and more importantly for the separation, is that the exoskeletons are in their early stages, and further research still needs to be conducted to ensure that the upper extremity exoskeleton and lower extremity exoskeleton can function well independently before we can venture an attempt to integrate them. See [5] for research work on upper extremity exoskeletons at Berkeley.

The concept of a powered human-assistive exoskeleton has been explored in various reach projects since the 1950's, though recent advances in controls and computation have generated renewed interest (see [6],[7],[8]). A recent notable project is the "RoboKnee," which is a powered knee brace that functions in parallel to the wearer's knee but does not transfer loads to the ground [9]. This device transfers the weight of the backpack payload onto the human skeleton (including shanks, ankles, and feet). "HAL", a walking aid system for individuals with gait disorders, is another current exoskeleton-like device in that it adds to the force generated by the human muscles but relies on the human skeleton to transfer loads [10]. BLEEX draws on this history of exoskeleton development but is unique in that it mechanically functions as a true load bearing exoskeleton, is energetically autonomous, and utilizes a unique control system that does not require any direct measurements on the human.

Networked control systems (NCSs), such as the one developed for BLEEX, have broad applications beyond just exoskeleton control and have been adopted in fields related to industrial automation, building automation, office and home automation, intelligent vehicles, aircrafts, and spacecrafts [11],[12],[13]. Several network types had been developed based upon the applications, such as a process field bus (PROFIBUS) [14], manufacturing automation protocol (MAP) [15], and fiber distributed data interface (FDDI) [16]. EtherNet, ControlNet, and DeviceNet are some other common NCSs that are compared as control networks in different situations and schemes in [17].

III. SENSITIVITY AMPLIFICATION CONTROLLER

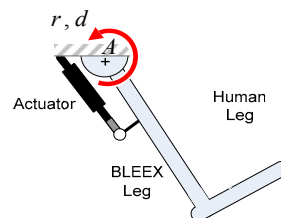### A. A simple One Degree-of-Freedom (DOF) Example

Fig. 2 One DOF model of an exoskeleton leg interacting with the pilot's leg.

The control of the exoskeleton is explained here through the 1 DOF example shown in Fig. 2. This figure schematically depicts a human leg attached and interacting with a 1 DOF exoskeleton leg in a swing configuration (no interaction with the ground). The exoskeleton leg is represented as a rigid link

pivoting about a single revolute joint at the hip and powered by a single actuator. The exoskeleton leg in this example has an actuator that produces a torque, r, about pivot point A.

Although the pilot is attached securely to the exoskeleton at the foot, other parts of the pilot leg, such as the shanks and thighs, can contact the exoskeleton and impose forces and torques on the exoskeleton leg. The equivalent torque on the exoskeleton leg, resulting from the pilot's applied forces and torques, is represented by d.

In the case where multiple actuators produce controlled torques on the system, r would become a vector of torques imposed on the exoskeleton by the actuators. G is the transfer function from the actuator input, r, to the exoskeleton angular velocity, v (actuator dynamics are included in G). The form of G and the type of internal feedback for the actuator is immaterial for the discussion here. The Laplace operator has been omitted in all equations for the sake of compactness.

The sensitivity transfer function S, represents how the equivalent human torque affects the exoskeleton angular velocity. S maps the equivalent pilot torque, d, onto the exoskeleton velocity, v. If the actuator already has some sort of primary stabilizing controller, the magnitude of S will be small and the exoskeleton will only have a small response to the imposed forces and torques from the pilot or any other source. For example, a high gain velocity controller in the actuator results in small S, and consequently a small exoskeleton response to forces and torques. Also, non-backdrivable actuators (e.g. large transmission ratios or servo-valves with overlapping spools) result in a small S which leads to a correspondingly small response to pilot forces and torques.

The resulting torque from pilot on the exoskeleton, d, is not an exogenous input; it is a function of the pilot dynamics and variables such as position and velocity of the pilot and the exoskeleton legs. These dynamics change from person to person, and within a person as a function of time and posture. These dynamics will be added to the analysis in later paragraphs, but they are unrelated to the purpose of current discussion.

Our goal is to develop an exoskeleton with a large sensitivity to forces and torques from the operator using measurements only from the exoskeleton (i.e. no sensors on the pilot or the exoskeleton interface with the pilot).

Creating a negative feedback loop from the exoskeleton variables only, the closed-loop sensitivity transfer function is presented in (1).

$$S_{NEW} = \frac{v}{d} = \frac{S}{1 + GC} \tag{1}$$

Observation of (1) reveals that $S_{NEW} \leq S$, and therefore any negative feedback from the exoskeleton leads to an even smaller sensitivity transfer function. With respect to (1), our goal is to design a controller for a given S and G such that the closed loop response from d to v (the new sensitivity function as given by (1)) is greater than the open loop sensitivity transfer function (i.e. S) within some bounded frequency range. This design specification is given by inequality (2).

$$|S_{NEW}| > |S| \qquad \forall \omega \in (0, \omega_O) \tag{2}$$

or alternatively $|1 + GC| < 1 \quad \forall \omega \in (0, \omega_O)$ (3)

where ω_O is the exoskeleton maneuvering bandwidth.

Exoskeleton control requires a totally opposite goal from classical and modern control theory: *maximize the sensitivity of the closed loop system to forces and torques*. In classical servo problems, negative feedback loops with large gains result in small sensitivity within a bandwidth, which means that they reject forces and torques (usually called disturbances). However, the above analysis states that the exoskeleton controller needs a large sensitivity to forces and torques.

The exoskeleton controller uses the inverse of the exoskeleton dynamics as a positive feedback such that the loop gain for the exoskeleton approaches unity from below (slightly less than 1), which can be written as:

$$S_{NEW} = \frac{v}{d} = \frac{S}{1 - GC} \tag{4}$$

where C is chosen as $C = \left(1 - \alpha^{-1}\right) G^{-1}$ (5)

and α is the amplification number greater than unity.

If $\alpha = 10$, then $C = 0.9 G^{-1}$, and the new sensitivity transfer function is $S_{NEW} = 10S$ (ten times the force amplification). Equation (5) simply states that a positive feedback controller needs to be chosen as the inverse dynamics of the system dynamics scaled down by $(1 - \alpha^{-1})$. Note that (5) prescribes the controller in the absence of unmodeled high-frequency exoskeleton dynamics. In practice, C also includes a unity gain low pass filter to attenuate the unmodeled high-frequency exoskeleton dynamics that may not be captured in the model, G^{-1}.

The success of this control method is dependant on the accuracy of system model (i.e. G^{-1}) which governs how much torque is needed at each joint to compensate for the payload and dynamics of the exoskeleton. Models errors which cause the exoskeleton to apply too little actuation torque mean that the pilot would feel a portion of the payload. Errors which cause over-actuation however, could lead to instability. This straightforward control solution comes with an expensive price: robustness to parameter variations. To get the above method working, one needs to know the dynamics of the system very well. The next section discusses this tradeoff.

B. Robustness to Parameter Variations

The variation in the new positive feedback sensitivity transfer function (4) is given by

$$\frac{\Delta S_{NEW}}{S_{NEW}} = \frac{\Delta S}{S} + \frac{GC}{1 - GC} \frac{\Delta G}{G}. \tag{6}$$

If GC is close to unity (when the force amplification number, α, is large) any parameter variation on modeling will

be amplified as well. For example if the parameter uncertainty in the system is about 10%, i.e.:

$\left| \dfrac{\Delta G}{G} \right| = 0.10$ and $\left| \dfrac{\Delta S}{S} \right| = 0$, then (6) results in

$$\left| \frac{\Delta S_{NEW}}{S_{NEW}} \right| = \left| \frac{GC}{1 - GC} \right| 0.10 \tag{7}$$

Now assume C is chosen such that $C = 0.9G^{-1}$. Substituting into (7) results in $\left| \dfrac{\Delta S_{NEW}}{S_{NEW}} \right| = 0.90$. (8)

Equation (8) indicates that any parameter variation directly affects the system behavior. In the above example, a 10% error in model parameters results in nine times the variation in the sensitivity function. This is why model accuracy is crucial to exoskeleton control. One can see this problem as a tradeoff: the design approach described above requires no sensor (e.g. force or electromyogram) in the interface between the pilot and the exoskeleton; one can push and pull against the exoskeleton in any direction and at any location without measuring any variables on the interface. However, the control method requires a very good model of the system. At this time, our experiments with BLEEX have shown that this control scheme—which does not stabilize BLEEX—forces the exoskeleton to follow wide-bandwidth human maneuvers while carrying heavy loads.

C. Pilot Dynamics

In our control scheme, as will be shown, there is no need to include the internal components of the pilot limb model; the detailed dynamics of nerve conduction, muscle contraction, and central nervous system processing are implicitly accounted for in constructing the dynamic model of the pilot limbs. For more detail on in-depth modeling and analysis of the internal components of the pilot limb as applied to haptic systems and human power amplifiers, see [18],[19] and our preliminary results in [5].

The pilot force on the exoskeleton, d, is a function of both the pilot dynamics, H, and the kinematics of the pilot limb (e.g., velocity, position or a combination thereof).

$$d = -H(v) \tag{9}$$

The specific form of H is not known other than that it results in the human muscle force on the exoskeleton. In general, H is determined primarily by the physical properties of the human dynamics. Here we assume H is a nonlinear operator representing the pilot impedance as a function of the pilot kinematics.

Fig. 3 represents the closed loop system behavior when pilot dynamics are added. Examining Fig. 3 reveals that (4), representing the new exoskeleton sensitivity transfer function from d to v, is not affected by the feedback loop containing H.

Fig. 3 shows an important characteristic for human exoskeleton control: *two distinct feedback loops in the system*. The upper feedback loop represents how forces and torques from the pilot affect the exoskeleton and is internal to the human. The lower loop shows how the controlled feedback loop affects the exoskeleton. While the lower feedback loop is

positive (potentially destabilizing), the upper human feedback loop stabilizes the overall system of pilot and exoskeleton taken as a whole.
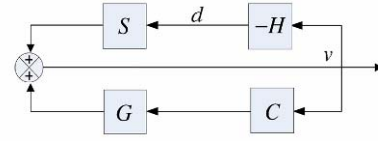

Fig. 3 The two feedback loops in this diagram represent the overall motion of the human and exoskeleton. The upper feedback loop shows how the pilot moves the exoskeleton through applied forces. The lower positive feedback loop shows how the controller drives the exoskeleton.

With the controller feedback loop with C added, the closed loop characteristic equation is

$$1 + SH - GC = 0. \tag{10}$$

Using the Small Gain Theorem, one can show that the closed loop stability is guaranteed as long as inequality (11) is satisfied.

$$|GC| < |1 + SH| \qquad \forall \omega \in (0, \infty) \tag{11}$$

Unlike control methods utilized in the control of the upper extremity exoskeletons [3], the human dynamics in the control method described here has little potential to destabilize the system. Even though the feedback loop containing C is positive, the feedback loop containing H stabilizes the overall system of pilot and exoskeleton. The condition in (11) could be violated if $|GC| \geq 1$, which would result from model parameter uncertainties. In summary, the controller discussed here is stable when worn by the pilot as long as parameter uncertainties are kept to a minimum. To ensure model accuracy, system identification experiments have been employed to validate calculated model parameters as reported in [4].

IV. CONTROLLER IMPLEMENTATION ON BLEEX

A. Mechanical system

The above discussion motivated the design philosophy using a one DOF system. BLEEX, as shown in Fig. 1, is a system with many degrees of freedom and therefore implementation of BLEEX control deserves further attention. Each BLEEX leg has three DOF at the hip, one DOF at the knee, and three DOF at the ankle, of which only four are powered DOF: hip, knee, and ankle joints in the sagittal plane and the hip abduction-adduction joints. See [20],[21] for details of the BLEEX mechanical design.

The pilot and BLEEX have rigid mechanical connections at the torso and the feet; everywhere else, the pilot and BLEEX have compliant or periodic contact. The connection at the torso is made using an adjustable compliant vest that distributes the forces between BLEEX and the pilot, thereby preventing abrasion. The vest includes a rigid plate (with hole pattern) on the back that bolts to the rigid metal spine of the BLEEX torso.

The pilot's shoes or boots attach to the BLEEX feet using a modified quick-release binding mechanism similar to snowboard bindings. The binding cleat on the modified pilot boot does not interfere with normal wear when the pilot is

unclipped from BLEEX. The BLEEX foot is composed of a rigid heel section with the binding and a compliant, but load bearing, toe section that begins mid foot and extends to the toe. The BLEEX foot has a compressible rubber sole with a tread pattern that provides both shock-absorption and traction while walking. The rubber sole of the BLEEX foot contains multiple embedded pressure sensors (coarse on/off information only), that are used to detect the trajectory of the BLEEX ground reaction force starting from "heel-strike" to "toe-off" in the walking gait cycle. This information is used in the BLEEX controller to identify the BLEEX foot configuration relative to the ground.

BLEEX is powered via a compact portable hybrid output power supply contained in the backpack. Several different portable BLEEX power supplies have been designed by our group for different applications and environments. Each provides hydraulic flow and pressure for the actuators and generates electric power for the sensors, network, and control computer. Details of the design, testing, and performance of the BLEEX power supplies can be found in [22].

B. Dynamic Modeling

Although biomechanical studies of walking frequently identify seven or more distinct phases of the human walking gait cycle (GC) [23], for simplicity in control we consider BLEEX to have three distinct phases (shown in Fig. 4) which manifest to three different dynamic models (percentage of GC indicated):

Single support: one leg is in the stance configuration while another leg is in swing (40% of GC).

Double support: both legs are in stance configuration and situated flat on the ground (20% of GC).

Double support with one redundancy: both legs are in stance configuration, but one leg is situated flat on the ground while the other one is not (40% of GC).

Using the information from the sensors in the foot sole, the controller determines which phase BLEEX is operating in and which of the three dynamic models apply.

In our initial control design process, we decoupled the control of the abduction-adduction DOF at the hip from the control of joints in the sagittal plane because we noticed through measurements that the abduction-adduction movements during normal walking (less than 0.9 m/s or 2 mph) are rather slow [20]. In comparison with the movements in the sagittal plane, the abduction-adduction movements could be considered quasi-static maneuvers with little dynamical affects on the rest of system. For the sake of brevity, the following sections describe the control method in the sagittal plane for a given set of abduction-adduction angles.
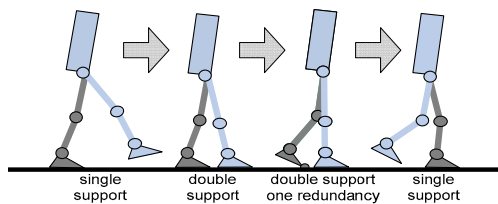

Fig. 4 Three phases of the BLEEX walking gait cycle.
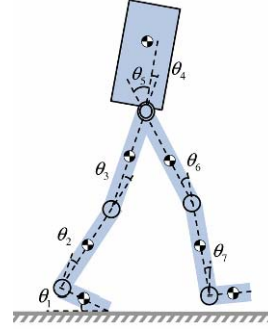
C. Single Support

Fig. 5 Sagittal plane representation of BLEEX in the single stance phase.

In the single support phase, BLEEX is modeled as the seven DOF serial link mechanism in the sagittal plane as shown in Fig. 5. The dynamics of BLEEX can be written in the general form as:

$$M(\theta)\ddot{\theta} + C(\theta,\dot{\theta})\dot{\theta} + P(\theta) = T + d \tag{12}$$

where $\theta = \begin{bmatrix} \theta_1 & \theta_2 & \dots & \theta_7 \end{bmatrix}^T$ and $T = \begin{bmatrix} 0 & T_1 & T_2 & \dots & T_6 \end{bmatrix}^T$.

M is a 7×7 inertia matrix and is a function of θ, $C(\theta,\dot{\theta})$ is a 7×7 centripetal and Coriolis matrix and is a function of θ and $\dot{\theta}$, and P is a 7×1 vector of gravitational torques and is a function of θ only. T is the 7×1 actuator torque vector with its first element set to zero since there is no actuator associated with joint angle θ_1 (i.e. angle between the BLEEX foot and the ground). d is the effective 7×1 torque vector imposed by the pilot on BLEEX at various locations. According to (5), we choose the controller to be the inverse of the BLEEX dynamics scaled by $(1 - \alpha^{-1})$, where α is the amplification number.

$$T = \hat{P}(\theta) + (1 - \alpha^{-1})\left[\hat{M}(\theta)\ddot{\theta} + \hat{C}(\theta,\dot{\theta})\dot{\theta}\right] \tag{13}$$

$\hat{C}(\theta,\dot{\theta})$, $\hat{P}(\theta)$ and $\hat{M}(\theta)$ are the estimates of the Coriolis matrix, gravity vector, and the inertia matrix respectively for the system shown in Fig. 5. Note that (13) results in a 7×1 actuator torque. Since there is no actuator between the BLEEX foot and the ground, the torque prescribed by the first element of T must be provided by the pilot. Substituting T from (13) into (12) yields,

$$M(\theta)\ddot{\theta} + C(\theta,\dot{\theta})\dot{\theta} + P(\theta) = \hat{P}(\theta) + (1 - \alpha^{-1})\left[\hat{M}(\theta)\ddot{\theta} + \hat{C}(\theta,\dot{\theta})\dot{\theta}\right] + d \tag{14}$$

In the limit when $M(\theta) = \hat{M}(\theta)$, $C(\theta,\dot{\theta}) = \hat{C}(\theta,\dot{\theta})$, $P(\theta) = \hat{P}(\theta)$, and α is sufficiently large, d will approach zero, meaning the pilot can walk as if BLEEX did not exist. However, it can be seen from (14) that the force felt by the pilot is a function of α and the accuracy of the estimates $\hat{C}(\theta,\dot{\theta})$, $\hat{P}(\theta)$, and $\hat{M}(\theta)$. In general, the more accurately the system is modeled, the less the human force, d, will be. In the presence of variations in abduction-adduction angles, only $P(\theta)$ in equations (13) and (14) needs to be modified.

D. Double Support

In the double support phase, both BLEEX feet are flat on the ground. The exoskeleton is modeled as two planar 3 DOF serial link mechanisms that are connected to each other along their uppermost link as shown in Fig. 6-a. The dynamics for these serial links are represented by (15) and (16).
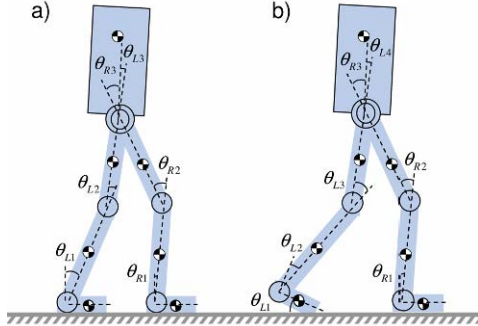

Fig. 6 Sagittal plane representation of BLEEX in a) the double support phase and b) the double support phase with one redundancy.

$$M_L(m_{TL},\theta_L)\ddot{\theta}_L + C_L(m_{TL},\dot{\theta}_L,\theta_L)\dot{\theta}_L +$$
$$P_L(m_{TL},\theta_L) = T_L + d_L \quad (15)$$

$$M_R(m_{TR},\theta_R)\ddot{\theta}_R + C_R(m_{TR},\dot{\theta}_R,\theta_R)\dot{\theta}_R +$$
$$P_R(m_{TR},\theta_R) = T_R + d_R \quad (16)$$

where: $\theta_L = \begin{bmatrix} \theta_{L1} & \theta_{L2} & \theta_{L3} \end{bmatrix}^T$ and $\theta_R = \begin{bmatrix} \theta_{R1} & \theta_{R2} & \theta_{R3} \end{bmatrix}^T$. m_{TR} and m_{TL} are effective torso masses supported by each leg and m_T is the total torso mass such that:

$$m_T = m_{TR} + m_{TL} \quad (17)$$

The contributions of m_T on each leg (i.e., m_{TL} and m_{TR}) are chosen as functions of the location of the torso center of mass relative to the locations of the ankles such that:

$$\frac{m_{TR}}{m_{TL}} = \frac{x_{TL}}{x_{TR}} \quad (18)$$

where x_{TL} is the horizontal distance between the torso center of mass and the left ankle, and x_{TR} is the horizontal distance between the torso center of mass and the right ankle. For example, if the center of mass of the torso is located directly above the right leg, then $m_{TL} = 0$ and $m_{TR} = m_T$. Similar to the single stance phase, the controllers are chosen such that

$$T_L = \hat{P}_L(m_{TL},\theta_L) +$$
$$(1 - \alpha^{-1})\left[\hat{M}_L(m_{TL},\theta_L)\ddot{\theta}_L + \hat{C}_L(m_{TL},\theta_L,\dot{\theta}_L)\dot{\theta}_L \right] \quad (19)$$

$$T_R = \hat{P}_R(m_{TR},\theta_R) +$$
$$(1 - \alpha^{-1})\left[\hat{M}_R(m_{TR},\theta_R)\ddot{\theta}_R + \hat{C}_R(m_{TR},\theta_R,\dot{\theta}_R)\dot{\theta}_R \right] \quad (20)$$

Needless to say, (18) is valid only for quasi-static conditions where the accelerations and velocities are small. This is in fact the case, since in the double support phase, both legs are on the ground and BLEEX's angular acceleration and velocities are quite small. This allows us to simplify (19) and

(20) during slow walking by removing all terms except the estimates of the gravitational vectors.

E. Double Support with One Redundancy

Double support with one redundancy is modeled as a three DOF serial link mechanism for the stance leg with the foot flat on the ground and a 4 DOF serial link mechanism for the stance leg that is not completely on the ground (Fig. 6-b). Each serial link supports a portion of the torso weight. The dynamics for these serial links are similar to (15) and (16), with the exception that the redundant leg equation represents four DOF as opposed to three. For the specific instant shown in Fig. 6-b, the left leg has 4 DOF and the right leg has 3 DOF.

Similar to the double support case, the effective torso mass supported by each leg is computed by (18). Controllers for this case can be chosen in the same manner as (19) and (20). Note that the actuator torque vector associated with the leg that has 4 DOF (e.g. T_L for the case shown in Fig. 6-b) is a 4×1 vector. As in the single support phase, the torque prescribed by the first element of T must be provided by the pilot because there is no actuator between the BLEEX foot and the ground. As the pilot walks, BLEEX transitions through the various phases shown in Fig. 4. The foot sole pressure sensors detect which leg has four degrees of freedom and which leg has three degrees of freedom and the controller then chooses the appropriate algorithm for each leg.

V. NETWORKED CONTROL SYSTEM

A. Network Structure

Fig. 7 provides global picture of the ExoNET networked control system that hosts the control algorithm. ExoNET was designed for BLEEX to enable the central controller to interact with distributed sensors, reduce the bulk, complexity, and difficulty of wiring, and achieve high-speed real-time control.

ExoNET consists of four ring networks (ExoRing0~3). Each ring consists of a chain of sensor and actuator data aggregation network nodes we call Remote I/O Modules, or RIOMs. Also, an additional network (GuiRing) provides an external PC based graphical user interface (GUI) for debugging that can be hot-swapped into the system while the network is running.

These five networks are all served by a central module (ExoBrain) composed of a single board computer (ExoCPU), a PCI Interface Module (ExoPCI) and a Supervisor I/O Module (SIOM). The SIOM is a custom built circuit board that has three independent transceiver channels that communicate with the GUI and ring networks. Transceiver channel 1 contains the two leg network rings: ExoRing0 and ExoRing2. Channel 2 contains the two torso network rings: ExoRing1 and ExoRing3. The third transceiver channel is coupled to GUI network (GuiRing).

The GUI network allows for real-time monitoring and administration of the control system from an external desktop PC for debugging purposes. The GUI network includes the GUI RIOM (GuiRIOM), the GUI PCI interface module

(GuiPCI) and the GUI computer (GuiPC) inside the GUI computer case. The GuiRIOM and the GuiPCI stack together on a PCI riser card that is plugged into one of PCI slots of the GuiPC.
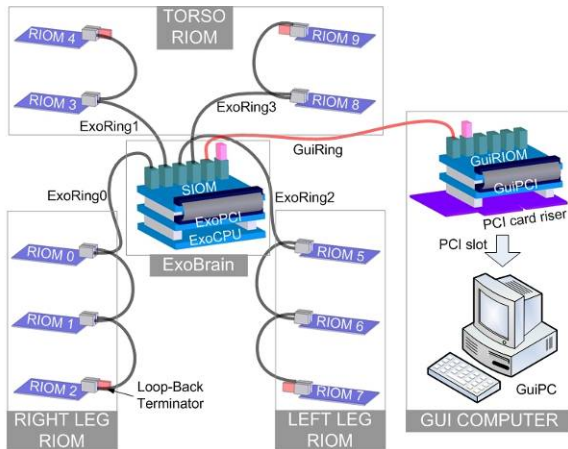

Fig. 7 Overall view of ExoNET networked control system and external GUI debug terminal.

Fig. 8 shows the ExoNET ring topology of an ExoRing where *N* RIOMs (Slave 1,2,…*N*) are serially connected to one SIOM (Master). Each serial link consists of three twisted pairs of wires. The first and second pairs are used for receiving and transmitting data and the third pair is used for carrying power to RIOMs. The direction of data flow in this network is from the transmit port (TX) of the master node to the receive port (RX) of the Slave 1 node, and from the TX of the Slave 1 node to the RX of the Slave 2 node, and so forth. This path continues to the RX of the Slave *N* node. A loop-back terminator completes the ring by plugging into the TX of the Slave *N* node so that data leaving from the TX of the Slave *N* node will arrive at the RX of the SIOM master node after passing through each slave node internal loop line (labeled LP in Fig. 8).
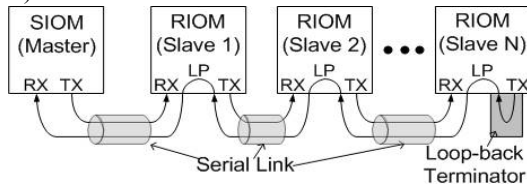

Fig. 8 Ring Topology

This ring topology provides flexibility and expandability for the network: a user can easily add or remove slave nodes and then plug a loop-back terminator at the last slave node to complete the network. This topology eliminates the requirement of a single circulating serial cable connecting from the last slave node to the master node. It is particularly useful in cabling a network where all nodes are physically oriented on a line (as on the BLEEX legs). In this case, only one serial link cable between any two consecutive nodes and a loop-back terminator on the last node are required to form a complete ring network.

B. Remote I/O Modules (RIOMS) – A Practical Solution to Managing Wiring Complexity

The ExoNET RIOM modules (Fig. 9) act as smart sensor and control data aggregation nodes. BLEEX is a complex multi-degree of freedom device with a large number of sensor inputs and control outputs. A common approach in robotic design would be to route all sensor and actuator signal wires directly to a central control computer. For BLEEX, this would have meant a total of over 210 wires. By distributing network nodes around the robot, we only require one wire per limb (i.e. ring network) to route all sensor and actuation information. Each node takes care of interfacing with the various types of sensors (serial, parallel, analog, digital, etc…) located physically close to it, and assembles the data into digital packets that can be transmitted via the network to and from the central computer. In addition, the RIOM can send out analog control commands for actuation (e.g. controlling a hydraulic servo-valve). The distribution and location of RIOMs is generally chosen to achieve a minimum volume of wiring and a reasonable and convenient allocation of sensors and actuators to each RIOM.
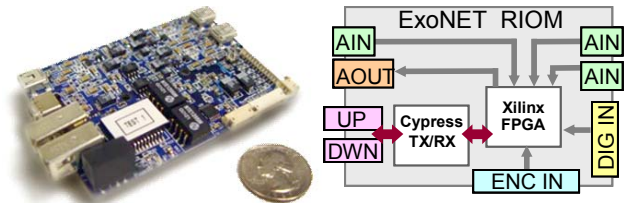

Fig. 9 ExoNET RIOM photo and schematic. Each RIOM provides for 3 analog inputs (AIN), 1 analog output (AOUT), 6 digital inputs (DIG IN), 1 quadrature encoder input (ENC IN), and 2 network communication ports (UP and DWN). Two integrated circuits handle processing (Xilinx Inc.) and network communication (Cypress Semiconductor Inc.) respectively.

Each RIOM on the first generation BLEEX provides for 5 sensor inputs and one 16-bit analog actuation output. Three of the inputs are 16-bit analog A/D converters used to read accelerometer data from the leg links and absolute angle inclinometer data from the torso. Each RIOM also has one quadrature encoder input for recording a relative joint angle and one 6-bit digital input used only on the foot RIOMs for measuring ground contact via foot switches. Details of the electronics hardware design can be found in [24].

C. Network Protocol

ExoNET network communication consists of passing data "messages" around the ring formed by the nodes on the network (SIOM and RIOMs). A message is a series of data packets that is preceded by a chosen start delimiter code ("S" in Fig. 10) and proceeded by a chosen end delimiter code ("E" in Fig. 10). Each data packet in a message includes bits that indicate the source of the packet (the ID# of a RIOM), the type of data (e.g. error, sensor, actuation command,…), the actual data value, and error checking bits based on a cyclic redundancy check (CRC). Fig. 10 shows two types of data packets in the message being passed between nodes: actuator commands sent from the master to the RIOMs (C1, C2), and sensor data destined for the master that was collected by the RIOMs (T11, T12, T21,…).

Each communication cycle in the network protocol (Fig. 9) involves passing a message sequentially from the master node (e.g. a SIOM) to each slave node in the ring network (e.g. the RIOMs) and then returning the message back to the master node. As the message travels around the ring, each RIOM reads its assigned actuator command data packet (by looking for its RIOM ID#), and then appends its locally collected sensor data to the message. When the message returns to the master (completing the ring), it has grown to include the sensor data from each node in the network. Because the communication cycles occur at a fixed rate set by the control scheme, this protocol allows for deterministic control and provides built in network error detection because every message returning to the master must contain information from every node on the ring.

Testing ExoNET on BLEEX has shown that the network update time for a ten RIOM network, passing 140 bytes of data, takes less than 20µs. The controller for BLEEX updates at 2 kHz (500 µs sample time), which leaves 480µs to perform the control algorithm calculations on the ExoCPU. For a more detailed discussion of the BLEEX control network and performance analysis, see [24],[25].
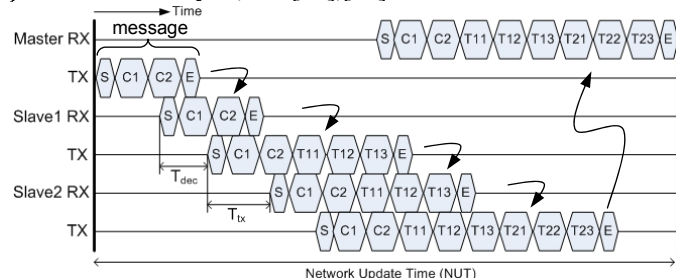

Fig. 10 Network communication overview. In a communication cycle, messages (strings of data packets beginning with start delimiter, S, and ending with end delimiter, E) pass from a master node (SIOM) to each slave node (RIOM) sequentially and return to the master node to complete the ring network communication. At each network node (horizontal line), the appropriate actuator command is read from the message and the local sensor data is appended before the message is passed down the ring.

VI. CONCLUSION

The Berkeley Lower Extremity Exoskeleton (BLEEX) is not a typical servo-mechanism in that it requires large sensitivity to pilot forces, which invalidates certain assumptions of the standard control design methodologies; thus, a new design approach was required. The controller described here uses the inverse dynamics of the exoskeleton as a positive feedback controller so that the loop gain for the exoskeleton approaches unity (slightly less than 1). Current experiments with BLEEX have shown that this control scheme has two superior characteristics: 1) it allows for wide bandwidth maneuvers; 2) it is unaffected by changing human dynamics. The trade off is that it requires a relatively accurate model of the system. We have addressed this trade off both through careful modeling of BLEEX hardware and system identification experiments to validate model parameters. The ExoNET control network that hosts the control algorithm is also presented. Video clips which demonstrate BLEEX, the control network, and the effectiveness of the control scheme can be found at http://bleex.me.berkeley.edu/bleex.

REFERENCES

[1] H. Kazerooni, J.L. Racine, H. Huang, and R. Steger, "On the Control of the Berkeley Lower Extremity Exoskeleton (BLEEX)," IEEE Int. Conf. Robotics and Automation, Barcelona, Spain, Apr. 2005.
[2] H. Kazerooni, and J. Guo, "Human Extenders," ASME J. Dyn. Sys., Measurements, and Control, vol. 115, no. 2B, June 1993, pp 281-289.
[3] H. Kazerooni, and M. Her, "The Dynamics and Control of a Haptic Interface Device," IEEE Transactions on Robotics and Automation, vol. 10, no. 4, Aug. 1994, pp 453-464.
[4] J. Ghan, and H. Kazerooni, "System Identification for the Berkeley Lower Extremity Exoskeleton (BLEEX)," IEEE Int. Conf. on Robotics and Automation, Orlando, FL, May 2006.
[5] H. Kazerooni, "The Human Power Amplifier Technology at the University of California, Berkeley", Journal of Robotics and Autonomous Systems, vol. 19, 1996, pp. 179-187.
[6] B.J. Makinson, and General Electric Co., "Research and Development for Machine Augmentation of Human Strength and Endurance, Hardiman I Project," G.E. Report S-71-1056, Schenectady, NY, 1971.
[7] M. Vukobratovic, D. Hristic, and Z. Stojiljkovic, "Development of Active Anthropomorphic Exoskeletons," Medical and Biological Engineering, Jan. 1974, pp. 66-80.
[8] K. Yamamoto, K. Hyodo, M. Ishii, and T. Matsuo, "Development of Power Assisting Suit for Assistng Nurse Labor," JSME International Journal Series C., vol. 45, No. 3, Sep. 2002.
[9] J. Pratt, B. Krupp, C. Morse, and S. Collins, "The RoboKnee: An Exoskeleton for Enhancing Strength During Walking", IEEE Conf. on Robotics and Automation, New Orleans, Apr. 2004.
[10] H. Kawamoto, and Y. Sankai, "Power Assist System HAL-3 for gait Disorder Person", ICCHP, Austria, July 2002.
[11] S. Biegacki and D. VanGompel, "The application of DeviceNet in process control", ISA Trans, vol. 35, no.2, 1996, pp. 169-176.
[12] L.D. Gibson, "Autonomous control with peer-to-peer I/O networks", Sensors, vol. 12, no. 9. Sept. 1995, pp. 83-90.
[13] A. Ray, "Introduction to networking for integrated control systems", IEEE Contr. Syst. Mag., vol. 9, Jan. 1989, pp. 76-79.
[14] D. Song, T. Divoux, and F. Lepage, "Design of the distributed architecture of a machine-tool using FIP fieldbus", in Proc. IEEE ICASSAP, Los Alamitos, 1996, pp. 250-260.
[15] G. Cena, C. Demartini, and A. Valenzano, "On the performances of two popular fieldbuses," in Proc. IEEE Int. Workshop on Factory Communication Systems, Barcelona, Spain, Oct. 1997, pp. 177-186.
[16] J.D. Wheelis, "Process control communications: Token Bus, CSMA/CD, or Token Ring?" ISA Trans., vol. 32, no. 2, July 1993, pp. 193-198.
[17] F.-L. Lian, J.R. Moyne, and D.M. Tibury, "Performance evaluation of control networks: Ethernet, ControlNet, and DeviceNet", IEEE Control Systems Magazine, vol. 21, no. 1, Feb. 2001, pp. 66-83.
[18] D.R. Wilkie, "The relation between force and velocity in human muscle", J. Physiology, vol. K110, 1950, pp. 248-280.
[19] J.M. Winters, and L. Stark, "Analysis of fundamental human movement patterns through the use on in-depth antagonistic muscle models", IEEE Trans. on Biomed. Engr. vol. BME32, no. 10, 1985.
[20] A. Zoss and H. Kazerooni, "On the Mechanical Design of the Berkeley Lower Extemity Exoskeleton," IEEE IROS, Canada. Aug. 2005.
[21] A. Chu, H. Kazerooni, and A. Zoss, "On the Biomimetic Design of the Berkeley Lower Extremity Exoskeleton (BLEEX)", IEEE Int. Conf. on Robotics and Automation, Barcelona, Spain, April 2005.
[22] K. Amundsen, J. Raade, N. Harding, and H. Kazerooni, "Hybrid Hydraulic-Electric Power Unit for Field and Service Robots," IEEE IROS, Edmunton, Canada, Aug. 2005.
[23] J. Rose, and J.G. Gamble, Human Walking, Second Edition, Williams & Wilkins, Baltimore, 1994, p. 26.
[24] S. Kim, G. Anwar, and H. Kazerooni, "High-speed Communication Network for Controls with Application on the Exoskeleton", American Control Conference, Boston, June 2004.
[25] S. Kim, and H. Kazerooni, "High-speed Ring-Based Distributed Networked Control System for Real-Time Multivariable Applications," 2004 IMECE & RD&D Expo, Nov. 2004.